

# Cosmic Censorship in Sgr A\* and M87\*: Observationally Excluding Naked Singularities

AVERY E. BRODERICK<sup>1,2,3</sup> AND KIANA SALEHI<sup>1,2,3</sup>

<sup>1</sup>*Perimeter Institute for Theoretical Physics, 31 Caroline Street North, Waterloo, ON, N2L 2Y5, Canada*

<sup>2</sup>*Department of Physics and Astronomy, University of Waterloo, 200 University Avenue West, Waterloo, ON, N2L 3G1, Canada*

<sup>3</sup>*Waterloo Centre for Astrophysics, University of Waterloo, Waterloo, ON N2L 3G1 Canada*

## ABSTRACT

The imaging of Sagittarius A\* (Sgr A\*) and the supermassive black hole at the center of Messier 87 (M87\*) by the Event Horizon Telescope constrains the location and nature of emission from these objects. Coupled with flux limits from the near-infrared through the ultraviolet, the attendant size constraints provide strong evidence for the absence of an accretion-powered photosphere, and therefore for the existence of an event horizon about an astrophysical black hole. Here, we demonstrate that a broad class of naked singularities are also generically excluded, regardless of the nature and unknown physical impact of singularity itself, subject to a single weak assumption about locality. While we restrict our attention to static, spherically symmetric spacetimes, we are nevertheless able to exclude a large number of commonly invoked naked singularity spacetimes in this way.

*Keywords:* Gravitation, Naked singularities, Radio continuum emission, High energy astrophysics, Galactic center, Active galaxies, Strong gravitational lensing

## 1. INTRODUCTION

Singularities are synonymous with black holes, the inexorable final destination of accreting material, and their resolution is among the chief motivations of the search for a quantum theory of gravity. In the absence of such a theory, they remain a mystery, presenting an as yet unknown boundary condition for the spacetime and the fields that populate it, and a potential source of unknown physical effects. For these reasons, predicting the future development of a singular spacetime and its contents presents a significant challenge. Nevertheless, the possibility of creating naked singularities, i.e., singularities not hidden behind an event horizon, even if only in principle, by over-spinning or over-charging general relativistic black holes remains unsettling. Moreover, it remains unclear if it is possible to generate naked singularities from generic initial conditions in general relativity or alternate theories of gravity (see, e.g., Janis et al. 1968; Joshi et al. 2011, 2014).

The formal problems associated with naked singularities threaten to render general relativity on its own a poorly posed initial value theory. This unpalatable state of affairs may be ameliorated in the observable universe if all singularities were to be hidden behind horizons (i.e., within black holes or behind the cosmic hori-

zon). This idea, codified as the “cosmic censorship hypothesis” introduced by Penrose (1969), effectively ensures that no point within the universe that we can currently observe is within the future Cauchy development of any singularity, and therefore unaffected by its unknown properties. However, cosmic censorship remains unproven theoretically and is, therefore, currently only addressable experimentally.

Observational arguments for the existence of astrophysical event horizons have existed for two decades now. These typically invoke advection dominated accretion flows (ADAFs), and the more general class of radiatively inefficient accretion flows (RIAFs; Narayan et al. 1995, 1998; Blandford & Begelman 1999; Yuan & Narayan 2014). Such flows are theoretically anticipated for accretion rates well below the Eddington rate, i.e.,  $\dot{M} < 0.01\dot{M}_{\text{Edd}} = 2 \times 10^{-11} (M/10^9 M_{\odot}) M_{\odot} \text{ yr}^{-1}$ , due to the weak Coulomb coupling between the electrons (which efficiently radiate) and the much more massive ions (which liberate the vast majority of the gravitational binding energy; Narayan et al. 1998; Narayan & McClintock 2008; Yuan & Narayan 2014). RIAFs, therefore, necessarily advect a large fraction of  $\dot{M}c^2$  as kinetic energy toward the central object. Wherein an event horizon (or at least apparent horizon) is present, this kinetic energy is lost, deposited within the black hole and increasing its mass. However, in the absence of an event horizon, e.g., in the presence of a surface, this energy will typically be thermalized and radiated. While ther-

malization happens naturally in baryonic atmospheres, for compact surfaces it is guaranteed by strong lensing for sufficiently high-redshift surfaces (Broderick et al. 2009b).<sup>1</sup> The result is a thermal bump in the spectral energy distribution (SED), the temperature and luminosity of which is set by energy balance with  $\dot{M}$  (Narayan et al. 1997; Narayan & Heyl 2002; Narayan & McClintock 2008; Broderick et al. 2009b, 2015).

These thermal bumps are explicitly seen in the X-ray spectra of accreting neutron star X-ray binaries, there associated with emission from the boundary flow onto the stellar surface, and conspicuously absent in black hole X-ray binaries (Narayan et al. 1997; Narayan & Heyl 2002; McClintock et al. 2004; Narayan & McClintock 2008). Supplemented with a long history of panchromatic observations, a detailed effort to understand and model accretion and jet launching in active galactic nuclei (AGN), the strongest constraints on visible surface/photosphere emission have been produced using the low-luminosity AGN Sagittarius A\* (Sgr A\*) and Messier 87\* (M87\*) (Broderick et al. 2009b, 2015). Within these, the dominant systematic uncertainty was the size of the emitting surface; a large surface can be cooler and therefore escape detection by hiding underneath the bright emission at mm wavelengths from the much hotter accretion flow.

The Event Horizon Telescope (EHT) has effectively retired this uncertainty for Sgr A\* (Event Horizon Telescope Collaboration et al. 2022a,b,c,d,e,f, 2024a,b, hereafter Sgr A\* Paper I-Sgr A\* Paper VIII) and M87\* (Event Horizon Telescope Collaboration et al. 2019a,b,c,d,e,f, 2021a,b, 2023, hereafter M87\* Paper I-M87\* Paper IX) by directly imaging those sources on angular scales that resolve the putative event horizons. These images confirm (1) that unstable circular photon orbits exist through the existence of the central brightness depression, and (2) that the emission region on the scale of the circular photon orbit is fully consistent with that anticipated by accretion onto general relativistic black holes (for implications for black hole spacetimes beyond general relativity see Kocherlakota et al. 2021; Sgr A\* Paper VI; Broderick et al. 2023; Salehi et al. 2024). Thus it is, EHT observations combined with contemporaneous near-infrared (NIR), optical and ultraviolet (UV) flux limits that provide the strongest empirical evidence currently for the existence of astrophysical event horizons.

The above empirical case in favor of event horizons is predicated on some degree of regularity near where the horizon would be, and may fail in the presence of a naked singularity. For example, the unknown physical impact of the singularity itself on the accreting material may

prevent the creation of a thermal photosphere, or accreting baryonic matter may simply disappear upon impacting the singularity. Even should the accreted material remain for some time, the gravitational redshift may never be sufficiently high to support the argument that the emitting surface must approximately be in thermal equilibrium due to strong lensing.

Despite the inherent uncertainties, a number of authors have embarked on making theoretical predictions of the images from naked singularity spacetimes (Joshi et al. 2011; Virbhadra & Ellis 2002; Joshi et al. 2020; Eichhorn et al. 2023; Nguyen et al. 2023; Saurabh et al. 2024; Deliyiski et al. 2024; Mishra et al. 2024; Chen et al. 2024a). Typically, these images include a new family of lensed images, generated by in-going photon trajectories that would otherwise be captured by the black hole. On the basis of the excess interior flux such images would generate, EHT images of Sgr A\* have already been brought to bear on the existence of some naked singularity spacetimes (Sgr A\* Paper VI). Such limits presume that the intervening space between the singularity and the emission region is transparent, a potentially dubious assumption given the astrophysical properties of the EHT targets. However, that generic, initially in-going null geodesics escape the near-singularity region immediately raises the possibility of similar general behavior for timelike geodesics, and thus may impact the fate of the accreting baryonic material.

Given a single modest assumption about the physics of the singularity — the direct unknown physical consequences of the singularity appear only within a very small distance of the singularity itself (e.g., the Planck length) — we show that for a very broad class of naked singularity spacetimes that the creation of a dense baryonic (and thus thermal) atmosphere is inevitable. We demonstrate this existence explicitly for static, spherically symmetric, asymptotically flat spacetimes. For Sgr A\* and M87\* we further show that the existence of such an atmosphere is conclusively excluded, and therefore neither of these objects can harbor naked singularities.

We begin in Section 2 with a general discussion of static, spherically symmetric, asymptotically flat spacetimes exhibiting naked singularities, presenting a classification scheme that identifies where and why the spacetime is singular. In Section 3 we address the general behavior of null and timelike geodesics, and therefore the fate of accreting baryonic gas. The spectral signatures and observational constraints for Sgr A\* and M87\* appear in Section 4 and Section 5, respectively. Finally, we collect concluding remarks in Section 6. Unless otherwise stated we assume a metric signature of  $-+++$  and set  $G = c = 1$ .

<sup>1</sup> See Broderick & Narayan (2007) for an example where the surface does not thermalize rapidly, and the potential for constraints on the existence of such systems even in that case.

## 2. GENERAL STATIONARY SPHERICALLY SYMMETRIC NAKED SINGULARITIES

The metric of any spherically symmetric, asymptotically spacetime can be written as,

$$ds^2 = -N^2 dt^2 + \frac{B^2}{N^2} dr^2 + r^2 d\Omega^2, \quad (1)$$

where  $r$  is the areal radius, and  $N(r)$  and  $B(r)$  are arbitrary functions of radius that asymptote to unity as  $r \rightarrow \infty$ . Well-behaved event horizons exist wherever  $N(r) = 0$ ; where  $B(r) = \infty$  the coordinates becomes singular. We turn now to the conditions under which Equation 1 describes a spacetime with a naked singularity.

The Kretschmann scalar,  $K \equiv R_{abcd}R^{abcd}$ , for the spherically symmetric spacetime described by Equation 1 is given by

$$K = \left\{ \frac{1}{B} \left[ \frac{(N^2)'}{B} \right]' \right\}^2 + 2 \left\{ \frac{(N^2)'}{rB^2} \right\}^2 + 2 \left\{ \frac{1}{r} \left( \frac{N^2}{B^2} \right)' \right\}^2 + \left\{ \frac{1}{r^2} \left( 1 - \frac{N^2}{B^2} \right) \right\}^2, \quad (2)$$

(see, e.g., eqs. 14-18 of Gkigkitzis 2014). Singular behavior in  $K$  necessarily betrays spacetime singularities. Because in spherical symmetry,  $K$  is composed of the elements of the Reimann squared (the metric in Equation 1 is manifestly diagonal), the converse statement is true: all spacetime singularities will produce singular  $K$ . When  $B(r) = 1$  everywhere (which is often true), Equation 2 reduces to the more simple form,

$$K = (f'')^2 + \frac{4(f')^2}{r^2} + \frac{4f^2}{r^4}, \quad (3)$$

where  $f \equiv 1 - N^2$ . For Schwarzschild,  $f = 2M/r$ , and the above reduces to the well-known result,  $K = 48M^2/r^6$ , which is singular at  $r = 0$ .

Therefore, the conditions upon the free functions in Equation 1 for the spacetime to contain a naked singularity are:

1. At some radius (or collection of radii),  $r_*$ ,  $K$  becomes singular, implying that a spacetime singularity exists.

2. For the outermost singularity, at all  $r > r_*$   $N(r)$  and  $B(r)$  are finite positive-definite functions of radius.

### 2.1. Classification of Spherical Singularities

The condition that the spacetime is singular requires one of the four terms in Equation 2 diverge at some radius  $r_*$ . We classify such behaviors by their location and the lowest order of the derivative of the term that diverges. First, by location, there are two possibilities, **P**: If  $r_* = 0$ , the singularity is ‘‘point-like’’. This the only point-like singularity in spherical symmetry.

**S**: If  $r_* > 0$ , the singularity is ‘‘shell-like’’. All non-point-like singularities are shell-like in spherical symmetry.

Second, by the lowest order of the first term that diverges<sup>2</sup>,

- 0**:  $N^2/r^2B^2 \rightarrow \infty$  at  $r_*$ .
- 1**:  $N^2/r^2B^2$  is finite but  $(N^2/B^2)'/r \rightarrow \infty$  or  $(N^2)'/rB^2 \rightarrow \infty$  at  $r_*$ .
- 2**:  $N^2/r^2B^2$ ,  $(N^2/B^2)'/r$ , and  $(N^2)'/rB^2$  are finite but  $[(N^2)'/B]'/B \rightarrow \infty$  at  $r_*$ .

Thus a spacetime for which  $N^2/r^2B^2 \rightarrow \infty$  at  $r_* = 0$  is classified as P0. Note that if any higher-order derivative term diverges at the origin, then the zeroth must as well (see Appendix A), and thus P0 is the only kind of ‘‘point-like’’ singularity in spherically symmetric, static spacetimes.

We further subdivide the type-0 spacetimes based on what is responsible for the divergence of  $N^2/r^2B^2$ .

- z**: If  $N \rightarrow \infty$  at  $r_*$  faster than  $r^{-1}$ , and  $B^{-1}$  remains finite, we define this to be a ‘‘redshift’’-type singularity because the redshift  $(1+z = N^{-1})$  goes to zero at  $r_*$ .
- j**: If  $B \rightarrow 0$  at  $r_*$  while  $r$  and  $N$  remain finite, we define this to be a ‘‘Jacobian’’-type singularity because  $\sqrt{-g} = Br^2 \sin \theta$  goes to zero at  $r_*$ .
- r**: If  $r \rightarrow 0$  at  $r_*$  while  $B$  and  $N$  remain finite, we define this to be a ‘‘radial’’-type singularity, which necessarily only occurs for P0-type singularities.

<sup>2</sup> It is possible for a naked singularity to be type P0 but the first term that diverges is not the last term in Equation 2 if  $\lim_{r \rightarrow 0} N^2/B^2 = 1$ . Nevertheless, supplemented with the condition that a singularity does, in fact, exist, this does not present a significant confusion.

Table 1. Example Spacetimes with Naked Singularities

Name	Type	$N^2(r)$	$B^2(r)$	Null/Weak	Param. range	Reference
RN	P0z	$1 - \frac{2M}{r} + \frac{Q^2}{r^2}$	1	Y/Y	$ Q  > M$	Reissner (1916)
SHRN	P0z	$1 - \frac{2M}{r} + \frac{Q^2 + s}{r^2}$	1	Y/Y	$Q^2 + s > M^2$	Astorino (2013)
EMD-1	P0z	$1 - \frac{\sqrt{4M^2 r^2 + q^4} - q^2}{r^2}$	$\frac{4r^2}{4r^2 + q^4}$	Y/Y	$q > \sqrt{2}$	Kocherlakota & Rezzolla (2020)
E ae-1	P0z	$1 - \frac{2M}{r} - \frac{27M^4 c_{13}}{16(1 - c_{13})r^4}$	1	Y/Y	$c_{13} < 0$ or $c_{13} > 1$	Kocherlakota & Rezzolla (2020)
E ae-2	P0z	$1 - \frac{(2 - c_{14})M}{r} - \frac{(2c_{13} - c_{14})(2 - c_{14})^2 M^2}{8(1 - c_{13})r^2}$	1	Y/Y	$\frac{2c_{13} - c_{14}}{1 - c_{13}} < -8$	Kocherlakota & Rezzolla (2020)
EEH	P0z	$1 - \frac{2M}{r} + \frac{q_m^2}{r^2} - \alpha \frac{2q_m^4}{5r^6}$	1	Y/Y	$\alpha \leq 0, q_m^2 > M^2$	Yajima & Tamaki (2001)
JNW <sup>a</sup>	P0z/r	$\left(1 - \frac{2M}{(1 - \nu)s}\right)^{1 - \nu}$	$\left(1 - \frac{2M}{(1 - \nu)s}\right)^{2 - \nu}$	Y/Y	$\nu > 1$ or $0 < \nu < 1$	Janis et al. (1968)
JMN-1	P0r	$-\left(1 - \frac{2M}{R_b}\right) \left(\frac{r}{R_b}\right)^{2M/(R_b - 2M)}$	$\left(\frac{r}{R_b}\right)^{2M/(R_b - 2M)}$	Y/Y	$0 \leq M \leq 2R_b/5$	Joshi et al. (2011)
JMN-2	P0r	$\left[\frac{(1 + \lambda)^2}{4\lambda\sqrt{2 - \lambda^2}} \left(\frac{r}{R_b}\right)^{1 - \lambda} - \frac{(1 - \lambda)^2}{4\lambda\sqrt{2 - \lambda^2}} \left(\frac{r}{R_b}\right)^{1 + \lambda}\right]^2$	$(2 - \lambda^2)N^2(r)$	Y/Y	$0 \leq \lambda < 1$ and $R_b > 0$	Joshi et al. (2014)
BST <sup>b</sup>	P0r	$\frac{2\beta^2}{1 + R_b/r}$	$N^2(r)/\beta^2$	$\beta^2 \leq \frac{12}{13}/\beta^2 \leq \frac{2}{3}$	$\beta, R_b \neq 0$	Banik et al. (2017)
BINS <sup>c</sup>	P0z	$1 - \frac{2M}{r} - \frac{2\bar{Q}^2}{3r^2 + 3\sqrt{r^4 + a\bar{Q}^2} + a\bar{Q}^2} + \frac{4\bar{Q}^2}{3r^2} \bar{F}\left(\frac{a\bar{Q}^2}{r^4}\right)$	1	Y/Y	$a < 4\bar{Q}^2$ and $M < M_e(a, \bar{Q})$	Chen et al. (2024b)
CNS	P0z	$\left(1 + \frac{M}{r}\right)^{-2} + \frac{Q^2}{r^2}$	1	Y/Y	$Q \neq 0$	Viththani et al. (2024)
4D EGB	P0r	$1 + \frac{r^2}{2\gamma M^2} \left(1 - \sqrt{1 + \frac{8\gamma M^3}{r^3}}\right)$	1	Y/Y	$\gamma > 0$	Deliyski et al. (2024)
4D EGBQ	S1	$1 + \frac{r^2}{2\gamma M^2} \left(1 - \sqrt{1 + \frac{8\gamma M^3}{r^3} - \frac{4\gamma M^2 Q^2}{r^4}}\right)$	1	Y/Y	$ Q  > 0$ and $\gamma > 1 - Q^2/M^2$	Fernandes (2020)

<sup>a</sup>The function  $s$  is defined implicitly by  $r = s\{1 - 2M/[(1 - \nu)s]\}^{\nu/2}$ , where  $s \in [s_*, \infty)$  maps smoothly onto  $r \in [0, \infty)$ . Note that within the literature, the Janis-Newman-Winicour metric is also called the Fisher metric (Fisher 1999), the Wyman solution (Wyman 1981; Virbhadra 1997), and the Buchdahl spacetime (Buchdahl 1959; Bhadra & Nandi 2001).

<sup>b</sup>Note that for the Bertrand singular spacetime, when  $\beta = 1$  it is the second term in Equation 2 that is the lowest order term that diverges.

<sup>c</sup>Born-Infeld naked singularity. For compactness, we define  $\bar{F}(z) \equiv {}_2F_1(1/4, 1/2, 5/4; -z)$ , where  ${}_2F_1(\dots)$  is the Gaussian hypergeometric function, and  $M_e(a, \bar{Q}) \equiv [4\bar{Q}^2 - a + 8\bar{Q}^2 \bar{F}(16a\bar{Q}^2/(4\bar{Q}^2 - a)^2)]/6\sqrt{4\bar{Q}^2 - a}$ .

In the following, we will demonstrate many key ideas with the Reissner-Nordström spacetime, which has the virtue of having or not having an event horizon, depending on the electric charge,  $Q$ , for which

$$N^2(r) = 1 - \frac{2M}{r} + \frac{Q^2}{r^2}, \quad (4)$$

and  $B(r) = 1$ . The associated  $K$  is

$$K = \frac{48M^2}{r^6} - \frac{96MQ^2}{r^7} + \frac{56Q^4}{r^8}, \quad (5)$$

which is singular only at  $r_* = 0$ , and therefore is type P0. Because  $B = 1$  and  $N \approx Q^2/r^2$  near  $r = 0$ , this is further classified as P0z. When  $Q > M$  there is no event horizon and this metric provides a useful example. A number of other naked singularity spacetimes are collected in [Table 1](#), where their type,  $N^2$ ,  $B^2$ , relevant parameter ranges may be found.

### 2.2. Energy Conditions and Singular Spacetimes

For alternative gravity theories, the energy content of the spacetime may not be relevant. Nevertheless, within the context of general relativity (and theories that admit an equation of the form of the Einstein equation), the null and weak energy conditions can provide insight into which classes of singular spacetimes are relevant and which may be “sick”.

The consideration of energy conditions is motivated by [Hawking \(1992\)](#), which proves that closed timelike curves (CTCs) cannot be produced by classical fields in compact regions of non-singular spacetimes without violating the weak energy condition and conjectures that a similar condition holds for localized violations for quantum fields (the “chronology protection conjecture”). While [Hawking \(1992\)](#) does not apply in spacetime regions containing singularities, if we imagine that the naked singularity spacetime is the late-time evolution from non-singular initial conditions, then the weak energy condition is sufficient to ensure that CTCs do not appear prior to the singularity’s formation. Therefore, insofar as exotic matter (negative rest energy) and CTCs are unphysical, the null and weak energy conditions provide some guidance as to which spacetimes may be relevant (apart, of course, having a naked singularity!).

The Ricci tensor for the metric in [Equation 1](#) is diagonal and given by

$$\begin{aligned} R_t^t = R_r^r &= -\frac{1}{2r^2B} \left[ \frac{r^2(N^2)'}{B} \right] \\ R_\theta^\theta = R_\phi^\phi &= \frac{1}{r^2} - \frac{1}{r^2B} \left( \frac{rN^2}{B} \right)', \end{aligned} \quad (6)$$

from which we have the Ricci scalar is

$$R = -\frac{1}{r^2B} \left[ \frac{(r^2N^2)'}{B} \right]' + \frac{2}{r^2}. \quad (7)$$

The associated Einstein tensor is diagonal and given by

$$\begin{aligned} G_t^t = G_r^r &= \frac{1}{r^2B} \left( \frac{rN^2}{B} \right)' - \frac{1}{r^2} \\ G_\theta^\theta = G_\phi^\phi &= \frac{1}{2r^2B} \left[ \frac{r^2(N^2)'}{B} \right]', \end{aligned} \quad (8)$$

from which we may immediately obtain the stress-energy tensor via  $T_\nu^\mu = G_\nu^\mu/8\pi$ .

The weak and null energy conditions must be met by all observers within the relevant class. Because the spacetimes under consideration are spherical symmetric, without loss of generality, we restrict our attention to the equatorial plane, within which, we may write the momentum of an arbitrary observer as  $p_\mu = (-e, X_r, 0, \ell)$ , which must satisfy

$$p^\mu p_\mu = -\frac{e^2}{N^2} + \frac{B^2}{N^2} X_r^2 + \frac{\ell^2}{r^2} = -\mu^2, \quad (9)$$

where  $\mu > 0$  for timelike observers and  $\mu = 0$  for null observers. The statement of the null and weak energy conditions,  $p_\mu T_\nu^\mu p^\nu \geq 0$  for all  $p^\mu$ , becomes,

$$\begin{aligned} -\frac{\mu^2}{r^2} \left[ \frac{1}{B} \left( \frac{rN^2}{B} \right)' - 1 \right] \\ + \frac{\ell^2}{r^4} \left\{ \frac{1}{2B} \left[ \frac{r^4}{B} \left( \frac{N^2}{r^2} \right)' \right] + 1 \right\} \geq 0. \end{aligned} \quad (10)$$

That is, for the weak energy condition we require the coefficients of both  $\mu^2$  and  $\ell^2$  to be non-negative for all  $r > r_*$ , while for the null energy condition we require only the latter.

Again, it is instructive to consider the case when  $B(r) = 1$ , for which we find

$$8\pi p_\mu T_\nu^\mu p^\nu = \mu^2 \left( \frac{f}{r^2} + \frac{f'}{r} \right) + \frac{\ell^2}{r^2} \left( \frac{f}{r^2} - \frac{f''}{2} \right), \quad (11)$$

where  $f$  is defined as in [Equation 3](#). The weak energy condition requires, in this case, that  $f/r^2 + f'/r \geq 0$  and  $f/r^2 - f''/2 \geq 0$  at all  $r > r_*$ . The first implies that for spacetimes exhibiting S1-type naked singularities and that obey the weak energy condition,  $f'$  must diverge positively; were  $f'$  to diverge negatively,  $f/r$  must diverge as quickly, and the singularity would be of type S0. Similarly, the second implies that for spacetimes exhibiting S2-type naked singularities and that obey the weak and/or null energy condition,  $f''$  must diverge negatively (or be S0).

For our example spacetime, Reissner-Nordström, these conditions reduce to

$$\frac{f}{r^2} + \frac{f'}{r} = \frac{Q^2}{r^4} \geq 0 \quad \text{and} \quad \frac{f}{r^2} - \frac{f''}{2} = \frac{2Q^2}{r^4} \geq 0, \quad (12)$$

both of which are satisfied unconditionally. Therefore, the Reissner-Nordström spacetime satisfies the weak energy condition (and thus the null energy condition). In



Table 1, we note which naked singularity spacetimes pass which energy condition.

### 3. NULL AND TIMELIKE GEODESICS ABOUT SPHERICALLY SYMMETRIC NAKED SINGULARITIES

By definition, for a spacetime to contain a naked singularity, timelike geodesics that connect the singularity to infinity,  $i_+$ , must exist. This does not mean that all timelike geodesics must extend from negative timelike infinity,  $i_-$ , to  $i_+$ . Nor does it require that timelike geodesics not become generally trapped by the singularity itself. In practice, however, for all stationary, spherically symmetric spacetimes with naked singularities of type P0z, P0r, or S0z, neither of these problems appear. Apart from a set of finely tuned cases, comprising a set of measure zero in  $(e, \ell)$  (see below), generically null and timelike geodesics escape the near-singularity region in finite time. We now turn to demonstrating and quantifying these facts.

#### 3.1. Effective Potentials and Inner Turning Points

All of the spacetimes described by Equation 1 admit two constants of motion associated with the timelike and azimuthal symmetries. As done in Section 2.2, these are typically expressed in terms of an energy,  $p_t = e$ , and angular momentum,  $p_\phi = \ell$ . The spherical symmetry implies that all motion is planar, and without loss of generality we may restrict our attention to motion confined to the equatorial plane. Therefore, the final constant of motion is the effective mass of the underlying particle.

For photons, which are massless, the null condition is gives,

$$-\frac{e^2}{N^2} + \frac{B^2}{N^2} p^{r^2} + \frac{\ell^2}{r^2} = 0, \quad (13)$$

from which we have

$$p^{r^2} = \frac{1}{B^2} \left[ e^2 - \frac{N^2 \ell^2}{r^2} \right] = \frac{1}{B^2} [e^2 - V_{\text{eff}}^n(r, \ell)], \quad (14)$$

where  $V_{\text{eff}}^n(r, \ell) = N^2 \ell^2 / r^2$  is the effective potential for null particles. Whether or not photons will encounter an inner turning point, and therefore extend from  $\mathcal{S}_-$  to  $\mathcal{S}_+$ , depends on which class of singularity is present and the photon's angular momentum.

For all type-0z and type-0r singularities (i.e., P0r, P0z, and S0z),  $V_{\text{eff}}^n(r, \ell)$  diverges at  $r_*$  by definition, and therefore for any  $e$  and  $\ell \neq 0$ , by continuity and asymptotic flatness, there must exist some  $r > r_*$  at which  $p^{r^2} = 0$ , and hence photons generally encounter an inner turning point. For other types of singularities, the equation of motion of photons at the singularity may remain regular. We will focus our attention on the type P0r, P0z, and S0z singularities henceforth unless otherwise stated.

For massive particles, the equation of motion departs from that of photons by the introduction of the particle mass,  $m$ ,

$$p^{r^2} = \frac{1}{B^2} [e^2 - V_{\text{eff}}^t(r, \ell)], \quad (15)$$

where

$$V_{\text{eff}}^t(r, \ell) = V_{\text{eff}}^n(r, \ell) + N^2 m^2 \quad (16)$$

is the effective potential for massive particles. Because  $N^2$  is positive definite for all  $r > r_*$  (because the singularity is naked!)  $V_{\text{eff}}^t(r, \ell) > V_{\text{eff}}^n(r, \ell)$  generally. This has the significant consequence that anywhere photons encounter an inner turning point, massive particles with equal energy and angular momenta will do so as well at larger radii. Massive particles with lesser energy will encounter an inner turning point even further away from the singularity (see, e.g., the examples in Figure 1). This fact has important consequences for the astronomical phenomenology of accreting systems.

#### 3.2. Time Delays at Inner Turning Points

Having established that for the nakedly singular spacetimes of interest (P0r, P0z, and S0z) that all timelike geodesics with  $\ell \neq 0$  will encounter a radial turning point prior to the singularity, we now turn to the practical question of how long this process takes as measured by distant observers. Generally, the equations of motion for an outwardly moving massive particle are,

$$p^t = \frac{e}{N^2} \quad \text{and} \quad p^r = \sqrt{\frac{e^2 - V_{\text{eff}}^t(r, \ell)}{B^2}}. \quad (17)$$

from which we have the time to propagate from  $r$  inward to  $r_{\text{tp}}$  and back is, by symmetry,

$$\Delta t = 2 \int_{r_{\text{tp}}}^r dr \frac{p^t}{p^r} = 2 \int_{r_{\text{tp}}}^r dr \frac{eB}{N^2 \sqrt{e^2 - V_{\text{eff}}^t(r, \ell)}}. \quad (18)$$

For a black hole, the smallest value of  $N^2(r)$  sets the timescale by virtue of the gravitational redshift. Even in that case, the propagation time diverges only logarithmically with the maximum redshift (see Appendix B). For naked singularities,  $N^2(r)$  never vanishes outside of  $r_*$ , and thus it is the radical in the denominator, which vanishes at the turning point, that sets the propagation timescale for massive particles.

The integral in Equation 18 may be evaluated approximately by Taylor expanding the radical term about the turning point. That is, near  $r_{\text{tp}}$ ,

$$e^2 - V_{\text{eff}}^t(r, \ell) = V_{\text{eff}}^t{}'(r - r_{\text{tp}}) + \dots, \quad (19)$$

where  $V_{\text{eff}}^t{}'$  is the first derivative with respect to  $r$  of  $V_{\text{eff}}^t(r, \ell)$  evaluated at  $r_{\text{tp}}$  and we have suppressed the dependence on  $\ell$  for clarity and ignored the special case

in which  $V_{\text{eff}}^{t'}$  vanishes<sup>3</sup>. Therefore, the total time delay,

$$\Delta t \gtrsim \frac{eB(r_{\text{tp}})}{N^2(r_{\text{tp}})} \sqrt{\frac{r - r_{\text{tp}}}{V_{\text{eff}}^{t'}}}, \quad (20)$$

is explicitly bounded with respect to  $r_{\text{tp}}$  (in stark contrast to the behavior near horizons, which typically diverges logarithmically with the distance from the horizon, see Appendix B). Thus,  $\Delta t$  is generally finite, typically of order the light crossing time of the system.

#### 4. SPECTRAL SIGNATURES OF NAKED SINGULARITIES

Summarizing the previous section: P0r, P0z, and S0z singular spacetimes, infalling massive particles will generally encounter an inner turning point prior to reaching the singularity on a finite timescale as seen by a distant observer. Importantly, this goes beyond proving the existence of a family of outward-going timelike geodesics (which exist by definition for naked singularities), but rather proves that generic infalling timelike geodesics will necessarily exit the near-singularity region, avoiding the singularity altogether. This result has significant consequences for the spectral signatures of these spacetimes, set entirely by baryonic physics in the non-singular portion of the spacetime.

We fashion an argument similar to Broderick et al. (2009b) and Broderick et al. (2015), based upon the observed low-efficiency of the accretion flows in Sgr A\* and M87\*, and constraints at shorter wavelengths on the thermalization of the unradiated kinetic energy. This is predicated on four underlying assumptions and observations.

**1. The accretion flows on Sgr A\* and M87\* are radiatively inefficient.** That is, only a small fraction of the liberated gravitational binding energy is radiated during infall. For both sources this is both theoretically anticipated and observed. For objects with accretion rates below 0.1% Eddington, Coulomb scattering is insufficient to redistribute energy from the ions, which by virtue of their mass accrue the majority of the gravitational binding energy, and the electrons, responsible for the overwhelming majority of the emission (Narayan et al. 1995, 1998; Narayan & McClintock 2008; Yuan & Narayan 2014). As a result, the vast majority of the kinetic energy of the accreting material is advected towards the central object. In practice, the

<sup>3</sup> For a given a particle energy,  $e$ ,  $V_{\text{eff}}^{t'}$  will vanish at the turning point for orbits with angular momentum set by  $\ell = 2N(e^2 - N^2m^2)^{3/2} / [(N^2)'e^2]$ , where all quantities are evaluated at  $r_{\text{tp}}$ . For infinitesimally larger or smaller  $e$  and/or  $\ell$ ,  $V_{\text{eff}}^{t'} \neq 0$ . Because we will be interested in the behavior of distributions of massive particles (i.e., accretion flows), we will ignore higher order derivatives of  $V_{\text{eff}}^{t'}$  in the estimation of propagation timescales as such terms are relevant for at most a set of measure zero in  $(e, \ell)$ .

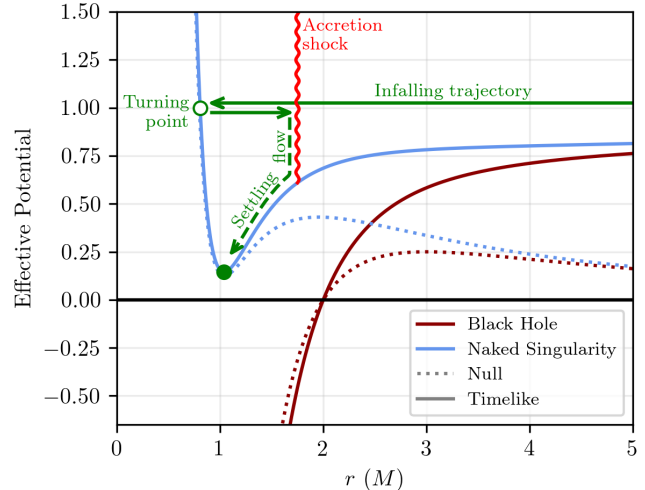


**Figure 1.** Null (dotted) and timelike (solid) effective potentials for Schwarzschild (dark red) and Reissner-Nordström (blue) spacetimes for  $Q = 1.01M$  and  $\ell = 0.5\sqrt{27}$ . The trajectory for an infalling particle with  $e = m$  at infinity is shown schematically in green, including the reflection at the inner turning point (open point), associated accretion shock when the outgoing and infalling flows collide, and the ultimate settling flow (dashed) depositing material at the potential minimum (solid point).

bolometric luminosity of Sgr A\* ( $\simeq 10^{36}$  erg s<sup>-1</sup>) and M87\* ( $\sim 10^{42}$  erg s<sup>-1</sup>) are well below estimates of  $\dot{M}c^2$  ( $\sim 3 \times 10^{38}$  erg s<sup>-1</sup> and  $10^{44}$  erg s<sup>-1</sup>, respectively), arrived at by Faraday rotation limits and EHT observations.

**2. Interaction between inflowing and outflowing accretion streams efficiently thermalizes bulk flows.** After encountering the near-singularity turning point, accreting gas will generate a local, if bound, outflow. For approximately axisymmetric accretion flows, which encompasses all models under consideration for Sgr A\* and M87\*, these outflows will collide with subsequently accreting gas, though potentially at a distinct azimuthal location. The resulting, relativistic counterstreaming gas flows are subject to multiple mechanisms for thermalizing their bulk energy, chief among which are shocks that will thermalize the energy on the shock-crossing time, which is less than or similar to the typical orbital timescale. Importantly, these dissipation mechanisms are dependent solely on the baryonic physics of the accreting material, and independent of the details of the singular spacetime. Thus, it is generally anticipated that the kinetic energy of the bulk flow fully thermalizes on very short timescales.

**3. The thermalized region remains compact.** Following thermalization, we will assume that the hot, thermalized region remains compact, i.e., smaller than the spacetime’s photon orbit (should one exist). This condition is a natural consequence of the very short ther-

malization timescale at the shocks, following which the gas will form into a settling flow toward the minimum of  $V_{\text{eff}}^t(r, 0)$ ,  $r_{\text{tp}, \text{min}}$  which is generally outside  $r_*$ . Moreover, in the cases of Sgr A\* and M87\*, the shadows observed by EHT indicate that the accretion flow remains well ordered down to the photon orbit, implying that any accretion shock must appear inside this region in those sources.

#### 4. The non-gravitational impact of the singularity is localized to its immediate neighborhood.

While the physics of the singularity is unknown, we presume that its non-gravitational influence is felt only by material within some small characteristic length scale,  $l_*$  (e.g., the Planck length). While it may be possible to engineer spacetimes with naked singularities with  $r_{\text{tp}, \text{min}} - r_* < l_*$ , such situations represent an extreme fine tuning and we do not consider them further.

Subject to the above, the general result is an optically thick, compact settling flow that efficiently radiates at a rate set by that at which energy is advected inward. That is, the luminosity and temperature as seen from a distant observer is

$$L_{\infty} = 4\pi R^2 \sigma T_{\infty}^4 \quad \text{and} \quad T_{\infty} = \left( \frac{\eta_{\text{ad}} \dot{M} c^2}{4\pi R^2 \sigma} \right)^{1/4}, \quad (21)$$

where  $\eta_{\text{ad}} \gtrsim 0.1$  is the fraction of the accreting rest mass energy that has liberated during infall that is advected into the settling flow,  $R$  is the radius of the black hole shadow, and  $\sigma$  is the Stefan-Boltzmann constant.

## 5. OBSERVATIONAL CONSTRAINTS

The general development of an optically thick, baryonic photosphere around a broad class of naked singularities (P0z, P0r, S0z) creates significant challenges for attempts to probe these spacetimes by looking for lensing signatures within the shadow (e.g., Sgr A\* Paper VI). Photons traveling on initially ingoing geodesics will be absorbed by the photosphere, which then prevents the additional lensing components from reaching distant observers. Nevertheless, strong empirical constraints on singular spacetime can be obtained by looking for the thermal emission from these photospheres directly.

Because  $T_{\infty}$  is set by  $\dot{M}$ , the associated thermal emission spectrum need not peak near 230 GHz, the frequency at which EHT observed Sgr A\* and M87\* in 2017 and 2018. Indeed, for the inferred accretion rates in those sources, it peaks at much higher frequency, with the consequence that EHT observations alone place only a weak constraint on the existence of an additional shock-heated thermal component. However, when the size constraints from EHT are supplemented with spectral flux measurements in the NIR, optical and UV, such a component can be excluded altogether. We now consider each target in turn, for which we summarize the state of the EHT observations and associated implied

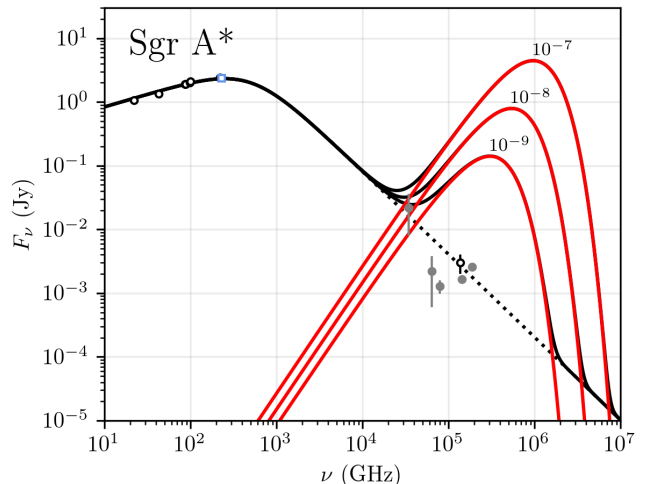


**Figure 2.** SED of Sgr A\* from a radially structured, non-thermal synchrotron emitting region (black dotted) and a thermal bump due to an optically thick settling flow (red) for  $\dot{M}$  ranging from  $10^{-9} M_{\odot} \text{ yr}^{-1}$  to  $10^{-7} M_{\odot} \text{ yr}^{-1}$ . For comparison, the 2017 EHT 230 GHz (1.3 mm) compact flux estimate (open blue square, Wielgus et al. 2022), contemporaneous broadband SED (open black points, Sgr A\* Paper II), and historical NIR upper limits from Broderick et al. (2009b) on the quiescent flux (gray closed points) are shown.

ranges for  $T_{\infty}$ , and compare to high-frequency flux measurements.

### 5.1. Sgr A\*

Sgr A\* is the bright radio source associated with the putative supermassive black hole at the center of the Milky Way. Its spectral energy distribution (SED), shown in Figure 2, is well described by a radiatively inefficient accretion flow that emits via synchrotron. Below a THz, Sgr A\* exhibits an inverted SED, with a spectral index ( $F_{\nu} \propto \nu^{-\alpha}$ ) of  $\alpha = -0.4$ , characteristic of a self-absorbed, radially structured synchrotron source (Blandford & Königl 1979; Broderick & Loeb 2006; Broderick et al. 2009a; Yuan et al. 2004; Sgr A\* Paper II). From near-infrared (NIR) through the X-ray wavelengths, Sgr A\*'s SED is well described by a power law with  $\alpha = 1.25$ , typical of optically thin nonthermal synchrotron sources (Sgr A\* Paper II).

The mass of and distance to Sgr A\* are the best known of any black hole candidate, established most accurately via the orbits of individual stars that pass within  $\sim 10^2\text{--}3$  AU of it, finding  $M = (4.297 \pm 0.013) \times 10^6 M_{\odot}$  and  $D = 8.277 \pm 34$  kpc (GRAVITY Collaboration et al. 2022; Do et al. 2019). However, that Sgr A\* is supermassive has been established in multiple ways. It lies at the center of a stellar cusp, the structure and dynamics of which require a supermassive central object (Genzel et al. 2010). It sits still very nearly at the minimum of the Galactic potential, with a velocity to



ward the North Galactic pole of  $-0.85 \pm 0.75 \text{ km s}^{-1}$ ; if this is the result of dynamical friction it requires  $M \gg 1 \times 10^6 M_\odot$  (Reid & Brunthaler 2020). Similarly, the distance to Sgr A\* has been further verified by direct parallax measurements of masers in the Galactic center (Reid et al. 2019). This mass and distance is fully consistent with that inferred by EHT through directly imaging the 1.3 mm emission on Schwarzschild scales, which found  $4.0_{-0.6}^{+1.1} \times 10^6 M_\odot$  (Sgr A\* Paper I; Sgr A\* Paper IV).

The EHT images of Sgr A\* provide at least three lines of strong evidence for the canonical near-virial accretion flow model. First, the presence of a dark shadow surrounded by a bright ring of emission matches quantitatively that anticipated by gravitational lensing about a  $4 \times 10^6 M_\odot$  black hole, and in particular the existence of a circular photon orbit (Sgr A\* Paper VI; Kocherlakota et al. 2021; Broderick et al. 2023). Second, the shape and amplitude of the power spectrum of brightness fluctuations matches those associated with the turbulence responsible for angular momentum transfer through the accretion flow in by general relativistic magnetohydrodynamic (GRMHD) simulations (Sgr A\* Paper V; Georgiev et al. 2022). Third, the linear polarization map is consistent with a predominantly toroidal magnetic field, again consistent with that anticipated by GRMHD simulations (Sgr A\* Paper VII; Sgr A\* Paper VIII; Broderick & Loeb 2006). Therefore, while the EHT images of Sgr A\* do not preclude any interior emission<sup>4</sup>, they do confirm the absence of any obstruction beyond the photon orbit.

At  $L = 10^{36} \text{ erg s}^{-1}$ , the total bolometric luminosity of Sgr A\* is well below its Eddington limit of  $6 \times 10^{44} \text{ erg s}^{-1}$ . Despite this, the high observed Faraday rotation measure implies cold plasma densities at distances of  $10M$ - $100M$  of  $10^6 \text{ cm}^{-3}$ , and corresponding to accretion rates of  $\dot{M} \sim 10^{-8} M_\odot \text{ yr}^{-1} \approx 10^{-7} \dot{M}_{\text{Edd}}$ , well into the RIAF regime (Agol 2000; Quataert & Gruzinov 2000; Marrone et al. 2007; Yuan & Narayan 2014). Similar conclusions follow from the direct modeling of the EHT images, which recover bolometric luminosities of  $7 - 9 \times 10^{35} \text{ erg s}^{-1}$  with associated accretion rates of  $0.5 - 1 \times 10^{-8} M_\odot \text{ yr}^{-1}$  (Sgr A\* Paper V). Thus, the empirically derived radiative efficiency is at most  $\eta \equiv L/\dot{M}c^2 \sim 10^{-3}$ , implying that the vast majority of the liberated gravitational potential energy is advected inward with the accretion flow.

From Equation 21, the temperature of an optically thick settling flow in Sgr A\* would be,

$$T_\infty \sim 10^4 \left( \frac{\eta_{\text{ad}}}{0.1} \right)^{1/4} \left( \frac{\dot{M}}{10^{-8} M_\odot \text{ yr}^{-1}} \right)^{1/4} \text{ K}, \quad (22)$$

<sup>4</sup> The EHT is sensitive only to emission with brightness temperatures exceeding  $\sim 10^8 \text{ K}$ , and thus would not be able to detect, e.g., the thermal emission from a settling flow surrounding a naked singularity (Broderick & Narayan 2006).

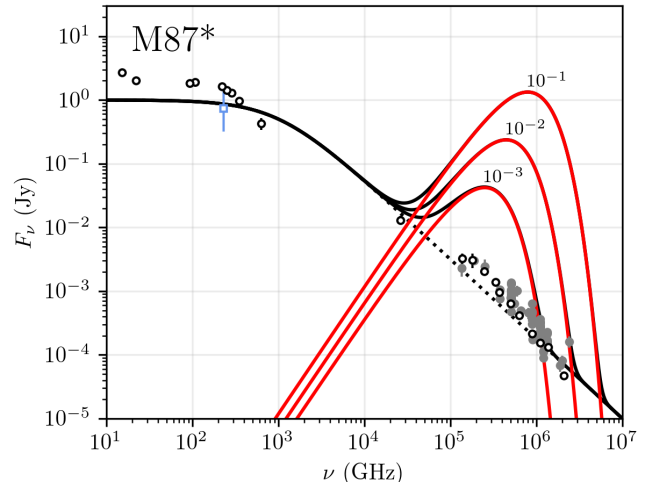


**Figure 3.** Spectral energy density of M87\* from a structured, non-thermal synchrotron emitting region (black dotted) and a thermal bump due to an optically thick settling flow (red) for  $\dot{M}$  ranging from  $10^{-3} M_\odot \text{ yr}^{-1}$  to  $10^{-1} M_\odot \text{ yr}^{-1}$ . For comparison, the 2017 EHT 230 GHz (1.3 mm) compact flux estimate (open blue square, M87\* Paper VI), contemporaneous broadband SED (open black points, EHT MWL Science Working Group et al. 2021), and historical NIR/Optical/UV fluxes from Broderick et al. (2015) (gray closed points) are shown.

which produces a thermal spectrum that peaks at optical wavelengths, shown for  $\eta_{\text{ad}} = 0.1$  and various  $\dot{M}$  in Figure 2.<sup>5</sup> For comparison, we also show the SED contemporaneous with the 2017 EHT observation campaign with a broken power-law fit approximating the self-absorbed synchrotron spectrum. We supplement these with the historical limits on the quiescent NIR flux listed in Table 2 of Broderick et al. (2009b). Optical flux estimates are not available due to the large extinction in the direction of the Galactic center. Nevertheless, the NIR flux limits conclusively exclude the existence of such an additional thermal component.

## 5.2. M87\*

The environment and behavior of M87\* differs from Sgr A\* in many relevant aspects. It is located at the center of the giant elliptical galaxy, Messier 87, which is itself among the brightest galaxies in the Virgo cluster (Zhu et al. 2014). A bright, broadband radio source, M87\* sits at the bottom of a prominent jet, a narrowly collimated relativistic outflow which extends to  $\sim 30 \text{ kpc}$  (de Gasperin et al. 2012). The origin of this jet is a topic of intense study, with both of the two main compet-

<sup>5</sup> Variations in the central mass (and thus  $R$ ) or the distance have negligible impact in comparison to the direct dependence on  $\dot{M}$  for both Sgr A\* and M87\*.

ing theoretical models powered by rotation and invoking twisted magnetic fields, either embedded within an orbiting accretion flow (Blandford & Payne 1982) or in a black hole horizon (Blandford & Znajek 1977)<sup>6</sup>. Both models require a surrounding accretion flow to source and confine the magnetic field, and thus  $\dot{M}$  is naturally related to the jet power.

Numerous independent estimates find a total jet power range of  $\sim 10^{44} \text{ erg s}^{-1}$ - $10^{45} \text{ erg s}^{-1}$  (see §2.2 of Broderick et al. 2015). These estimates range across physical scale, and therefore temporal delay, from the 30 kpc radio structure powered by the jet to HST-1, presumed to be powered by a jet shock (de Gasperin et al. 2012; Stawarz et al. 2006). This may be compared to  $\dot{M}$  inferred from jet launching models, which under conservative assumptions are related by

$$\dot{M} \gtrsim \frac{L_{\text{jet}}}{2c^2} \approx 10^{-3} M_{\odot} \text{ yr}^{-1}, \quad (23)$$

(see discussion in §2.1 of Broderick et al. 2015). This is in close agreement with the  $\dot{M}$  inferred from the Faraday rotation within the inner  $40M$ , assuming that the Faraday screen lies within an RIAF (Kuo et al. 2014).

The mass of M87\* has been measured primarily in two ways. First, via the dynamics of the orbiting stellar population as inferred from their cumulative spectra. This measurement is sensitive to assumptions regarding the dark matter cusp, and most recently found to be  $6.14_{-0.62}^{+1.07} \times 10^9 M_{\odot}$  (Gebhardt et al. 2011). Second, through the dynamics of orbiting gas, which has typically found much smaller masses (Walsh et al. 2013), though see Jeter et al. (2019) and Jeter & Broderick (2021). The larger, stellar dynamics mass is consistent with that inferred from the size of the bright ring observed by the EHT,  $M = (6.5 \pm 0.7) \times 10^9 M_{\odot}$ , and the one that we make use of here (M87\* Paper I; M87\* Paper VI). The distance is estimated either by using surface brightness fluctuations (Bird et al. 2010) or from the tip of the red giant branch (Blakeslee et al. 2009; Cantiello et al. 2018). We follow M87\* Paper VI and combine these to arrive at the estimate  $16.8_{-0.7}^{+0.8} \text{ Mpc}$ .

As with Sgr A\*, the EHT observations of M87\* are broadly consistent with the underlying astrophysical picture of the source. The brightness asymmetry is in good agreement with the dynamics of the orbiting material and the orientation of the jet on larger scales. The timescale over which EHT images of M87\* evolve is consistent with those found in GRMHD simulations, i.e., images of M87\* appear similar on neighboring days and differs on a week or longer (M87\* Paper IV; M87\* Paper V; Event Horizon Telescope Collaboration et al. 2024c). The magnetic field geometry of the jet footprint

in GRMHD simulations produces “twisty” linear polarization patterns that are quantitatively similar to that observed in EHT images (M87\* Paper VII; M87\* Paper VIII). The size of the inner shadow is indicative of the strong gravitational lensing at the circular photon orbit, and like Sgr A\*, provides strong evidence that there is no interfering settling flow outside of this radius.

The SED of M87\* is well described by a self-absorbed synchrotron jet source that transitions from optically thick to thin near a THz, shown in Figure 3 (Blandford & Königl 1979). Below the transition frequency, the SED is essentially flat ( $\alpha = 0$ ); above the transition the SED is well fit by a power law with  $\alpha = 1.25$ . The isotropic bolometric luminosity of M87\* is approximately  $10^{42} \text{ erg s}^{-1}$ , with the bulk of that appearing in the sub-mm (EHT MWL Science Working Group et al. 2021). Were this completely due to accretion, for  $\dot{M} = 10^{-3} M_{\odot} \text{ yr}^{-1}$ , the radiative efficiency would be  $\eta \sim 10^{-2}$ , reducing further if the jet is powered in part by some other source (e.g., spin of the naked singularity). These estimates are in good agreement with the GRMHD modeling of M87\* based on the EHT images, which find  $\dot{M}$  ranging from  $3 \times 10^{-2} M_{\odot} \text{ yr}^{-1}$  to  $10^{-4} M_{\odot} \text{ yr}^{-1}$  and an corresponding radiative efficiency range of  $10^{-4}$  to  $10^{-1}$  (M87\* Paper V). Thus, like in Sgr A\*, the majority of the liberated gravitational potential energy in M87\* is advected toward the black hole.

For M87\*, Equation 21 gives the equilibrium temperature for a putative optically thick settling flow to be

$$T_{\infty} \sim 4 \times 10^3 \left( \frac{\eta_{\text{ad}}}{0.1} \right)^{1/4} \left( \frac{\dot{M}}{10^{-3} M_{\odot} \text{ yr}^{-1}} \right)^{1/4} \text{ K}. \quad (24)$$

At this temperature, the associated thermal spectrum peaks in the NIR, though extends well into optical wavelengths. This is shown for various  $\dot{M}$  in Figure 3. Measurements of the SED of M87\* made contemporaneously with the 2017 EHT campaign are also shown, along with a broken power-law fit approximating a self-absorbed synchrotron source. We include the historical measurements from Broderick et al. (2015) to provide some sense of the variation with time.

Because M87\* is not obscured at optical and UV wavelengths, the measured SEDs extend across nearly the entire range of frequencies relevant for the thermal peak. Note that with the exception of the EHT compact flux measurement, all of the flux measurements are contaminated with emission from beyond  $10M$  (e.g., HST-1). Nevertheless, even with potential sizable contributions from outside the immediate vicinity of M87\*, the additional thermal component is conclusively excluded.

## 6. CONCLUSIONS

Naked singularities differ from other black hole foils in the potential for the introduction of unknown and uncontrolled physics, the effects of which must somehow

<sup>6</sup> The Blandford-Znajek model invokes black hole spin, and thus violates the underlying assumption of spherical symmetry. Nevertheless, we neglect spin further in our treatment here.

be circumscribed. Nevertheless, generally, a wide class of naked singularity spacetimes (P0z, P0r, and S0z) will contain inner turning points for timelike geodesics. As a result, accreting baryonic gas will reverse direction in a short time as seen far from the object, rapidly encounter subsequently accreting gas, shock, and ultimately produce a settling flow outside of the singularity. This process occurs entirely within the non-singular part of the spacetime on scales that have already been observed; that it is independent of the unknown physics at the singularity corresponds to the very modest assumption that the singularity's impact is confined to matter that comes within some small distance of it, e.g., comparable to the Planck length.

That accreting material impinging upon the settling flow will thermalize the remainder of its kinetic energy, i.e., that gained during infall, is guaranteed by known baryonic physics. Therefore, for this class of naked singularity spacetimes, an enveloping, optically thick, thermally emitting, photosphere, is an inevitable consequence. This photosphere may block initially ingoing null geodesics, rendering tests based on directly observing lensed emission inside the shadow challenging. However, for sources that are sufficiently radiatively inefficient and compact, this photosphere can be bright, and therefore its existence observationally probed.

Sgr A\* and M87\* satisfy both of these conditions. Both sources are radiatively inefficient, i.e., only a small fraction of the liberated gravitational potential energy is radiated. This is anticipated by theoretical models of the accretion process that have received significant empirical support from EHT observations and directly demonstrated via comparison of the source broadband luminosity to estimates of the accretion rate. EHT observations of both sources also constrains the distance at which departures can occur from a black hole accretion flow to within the circular photon orbit. That is, in both sources any putative baryonic photosphere would need to be compact.

The inferred  $\dot{M}$  in both sources would generate an emitting photosphere with a temperature, as measured by a distant observer,  $\sim 10^4$  K, and therefore peaking in the NIR, optical, or UV. The presence of such a thermal component can be conclusively excluded by flux measurements made contemporaneously with the EHT campaign in 2017. That is, neither Sgr A\* nor M87\* can be a type P0z, P0r, or S0z naked singularity spacetime. Practically, this set of classes encompass all but one of the asymptotically flat, spherically symmetric, naked singularity spacetimes that we could find in the literature (listed in Table 1).

There are at least three natural ways for naked singularities to evade the observational constraints we present. First, the singularity may be of a different type, i.e., S1, S2, or P0j. We note, however, that simply being a different type is not sufficient. While timelike geodesics in P0r, P0z, and S0z singular spacetimes have

generic behaviors that result in now-excluded observational consequences, it is clearly possible for other types of naked singularity spacetimes to do so. In Appendix C, we explicitly demonstrate that a type S1 naked singularity spacetime (and the only example we could find in the literature) may be excluded by the argument described here. Of course, we have also neglected any observable impact from the singularity itself.

Second, we have not considered the impact of spin. Neither the class of naked singularity spacetimes we exclude nor the specific examples listed in Table 1 are spinning. Nevertheless, the formal possibility remains that the introduction of spin may make qualitative differences in the strength of constraints. Incorporating spin complicates the question of the ultimate fate the accreting gas, substantially increasing of the size of the class of geodesics that must be surveyed. Therefore, We leave an investigation into general classes of spinning spacetimes for future work (e.g., that presented by Johannsen et al. 2016 and considered in Salehi et al. 2024).

Third, the unknown physics introduced by the singularity may include non-local interactions that extend past the inner turning point. Were this to be the case, the chief advantage of the constraints we present, that they derive wholly from non-singular regions within the spacetime, would be eliminated. However, we consider this situation to be a rather different problem.

Finally, while we have argued that neither Sgr A\* nor M87\* can harbor a naked singularity of the proscribed types, this says nothing about whether or not naked singularities can exist in other sources. Natural extensions of our argument can be made to other AGN and X-ray binaries in low-luminosity states (e.g., XTE J1118+480). The main limitation will be, in the absence of images that resolve the gravitational radius, the need for an additional assumption regarding the compactness of the putative additional thermal component. Nevertheless, future ground-based (Blackburn et al. 2019; Doeleman et al. 2023) and space-based arrays promise to extend the reach of direct imaging to a much larger population of sources (Pesce et al. 2021, 2022), and with it strong evidence excluding naked singularities in many additional sources.

1 We thank Aaron Held for helpful discussions on the potential of indirect detection of naked singularities. This  
 2 work was supported in part by Perimeter Institute for  
 3 Theoretical Physics. Research at Perimeter Institute is  
 4 supported by the Government of Canada through the  
 5 Department of Innovation, Science and Economic Development  
 6 Canada and by the Province of Ontario through  
 7 the Ministry of Economic Development, Job Creation  
 8 and Trade. A.E.B. receives additional financial support  
 9 from the Natural Sciences and Engineering Research  
 10 Council of Canada through a Discovery Grant.  
 11

## REFERENCES

- Agol, E. 2000, *ApJL*, 538, L121
- Astorino, M. 2013, *PhRvD*, 88, 104027
- Banik, U., Dey, D., Bhattacharya, K., & Sarkar, T. 2017, *General Relativity and Gravitation*, 49, 116
- Bhadra, A., & Nandi, K. K. 2001, *International Journal of Modern Physics A*, 16, 4543
- Bird, S., Harris, W. E., Blakeslee, J. P., & Flynn, C. 2010, *A&A*, 524, A71
- Blackburn, L., Doeleman, S., Dexter, J., et al. 2019, in *Bulletin of the American Astronomical Society*, Vol. 51, 256
- Blakeslee, J. P., Jordán, A., Mei, S., et al. 2009, *ApJ*, 694, 556
- Blandford, R. D., & Begelman, M. C. 1999, *MNRAS*, 303, L1
- Blandford, R. D., & Königl, A. 1979, *ApJ*, 232, 34
- Blandford, R. D., & Payne, D. G. 1982, *MNRAS*, 199, 883
- Blandford, R. D., & Znajek, R. L. 1977, *MNRAS*, 179, 433
- Broderick, A. E., Fish, V. L., Doeleman, S. S., & Loeb, A. 2009a, *ApJ*, 697, 45
- Broderick, A. E., & Loeb, A. 2006, *ApJL*, 636, L109
- Broderick, A. E., Loeb, A., & Narayan, R. 2009b, *ApJ*, 701, 1357
- Broderick, A. E., & Narayan, R. 2006, *ApJL*, 638, L21
- . 2007, *Classical and Quantum Gravity*, 24, 659
- Broderick, A. E., Narayan, R., Kormendy, J., et al. 2015, *ApJ*, 805, 179
- Broderick, A. E., Salehi, K., & Georgiev, B. 2023, *ApJ*, 958, 114
- Buchdahl, H. A. 1959, *Physical Review*, 115, 1325
- Cantiello, M., Blakeslee, J. P., Ferrarese, L., et al. 2018, *The Astrophysical Journal*, 856, 126
- Chen, Y., Wang, P., Wu, H., & Yang, H. 2024a, *JCAP*, 2024, 032
- . 2024b, *PhRvD*, 109, 084014
- de Gasperin, F., Orrú, E., Murgia, M., et al. 2012, *A&A*, 547, A56
- Deliyski, V., Gyulchev, G., Nedkova, P., & Yazadjiev, S. 2024, *arXiv e-prints*, arXiv:2401.14092
- Do, T., Hees, A., Ghez, A., et al. 2019, *Science*, 365, 664
- Doeleman, S. S., Barrett, J., Blackburn, L., et al. 2023, *Galaxies*, 11, 107
- EHT MWL Science Working Group, Algaba, J. C., Anczarski, J., et al. 2021, *ApJL*, 911, L11
- Eichhorn, A., Gold, R., & Held, A. 2023, *ApJ*, 950, 117
- Event Horizon Telescope Collaboration, Akiyama, K., Alberdi, A., et al. 2019a, *ApJL*, 875, L1
- . 2019b, *ApJL*, 875, L2
- . 2019c, *ApJL*, 875, L3
- . 2019d, *ApJL*, 875, L4
- . 2019e, *ApJL*, 875, L5
- . 2019f, *ApJL*, 875, L6
- . 2021a, *ApJL*, 910, L12
- . 2021b, *ApJL*, 910, L13
- . 2022a, *ApJL*, 930, L12
- . 2022b, *ApJL*, 930, L13
- . 2022c, *ApJL*, 930, L14
- . 2022d, *ApJL*, 930, L15
- . 2022e, *ApJL*, 930, L16
- . 2022f, *ApJL*, 930, L17
- . 2023, *ApJL*, 957, L20
- . 2024a, *ApJL*, 964, L25
- . 2024b, *ApJL*, 964, L26
- . 2024c, *A&A*, 681, A79
- Fernandes, P. G. S. 2020, *Physics Letters B*, 805, 135468
- Fisher, I. Z. 1999, *arXiv e-prints*, gr
- Gebhardt, K., Adams, J., Richstone, D., et al. 2011, *ApJ*, 729, 119
- Genzel, R., Eisenhauer, F., & Gillessen, S. 2010, *Rev. Mod. Phys.*, 82, 3121
- Georgiev, B., Pesce, D. W., Broderick, A. E., et al. 2022, *ApJL*, 930, L20
- Gkigkitzis. 2014, *Physics International*, 5, 103
- GRAVITY Collaboration, Abuter, R., Aymar, N., et al. 2022, *A&A*, 657, L12
- Hawking, S. W. 1992, *PhRvD*, 46, 603
- Janis, A. I., Newman, E. T., & Winicour, J. 1968, *PhRvL*, 20, 878
- Jeter, B., & Broderick, A. E. 2021, *ApJ*, 908, 139
- Jeter, B., Broderick, A. E., & McNamara, B. R. 2019, *ApJ*, 882, 82
- Johannsen, T., Wang, C., Broderick, A. E., et al. 2016, *Physical Review Letters*, 117, 091101
- Joshi, A. B., Dey, D., Joshi, P. S., & Bambhaniya, P. 2020, *PhRvD*, 102, 024022
- Joshi, P. S., Malafarina, D., & Narayan, R. 2011, *Classical and Quantum Gravity*, 28, 235018
- . 2014, *Classical and Quantum Gravity*, 31, 015002
- Kocherlakota, P., & Rezzolla, L. 2020, *PhRvD*, 102, 064058
- Kocherlakota, P., Rezzolla, L., Falcke, H., et al. 2021, *PhRvD*, 103, 104047
- Kuo, C. Y., Asada, K., Rao, R., et al. 2014, *ApJL*, 783, L33
- Marrone, D. P., Moran, J. M., Zhao, J.-H., & Rao, R. 2007, *ApJL*, 654, L57
- McClintock, J. E., Narayan, R., & Rybicki, G. B. 2004, *ApJ*, 615, 402
- Mishra, R., Vieira, R. S. S., & Kluźniak, W. 2024, *MNRAS*, 530, 3038

- Narayan, R., Garcia, M. R., & McClintock, J. E. 1997, *ApJL*, 478, L79
- Narayan, R., & Heyl, J. S. 2002, *ApJL*, 574, L139
- Narayan, R., Mahadevan, R., Grindlay, J. E., Popham, R. G., & Gammie, C. 1998, *ApJ*, 492, 554
- Narayan, R., & McClintock, J. E. 2008, *NewAR*, 51, 733
- Narayan, R., Yi, I., & Mahadevan, R. 1995, *Nature*, 374, 623
- Nguyen, B., Christian, P., & Chan, C.-k. 2023, *ApJ*, 954, 78
- Penrose, R. 1969, *Nuovo Cimento Rivista Serie*, 1, 252
- Pesce, D. W., Palumbo, D. C. M., Ricarte, A., et al. 2022, *Galaxies*, 10, 109
- Pesce, D. W., Palumbo, D. C. M., Narayan, R., et al. 2021, *ApJ*, 923, 260
- Quataert, E., & Gruzinov, A. 2000, *ApJ*, 545, 842
- Reid, M. J., & Brunthaler, A. 2020, *ApJ*, 892, 39
- Reid, M. J., Menten, K. M., Brunthaler, A., et al. 2019, *ApJ*, 885, 131
- Reissner, H. 1916, *Annalen der Physik*, 355, 106
- Salehi, K., Broderick, A. E., & Georgiev, B. 2024, *ApJ*, 966, 143
- Saurabh, Bambhaniya, P., & Joshi, P. S. 2024, *A&A*, 682, A113
- Stawarz, L., Aharonian, F., Kataoka, J., et al. 2006, *MNRAS*, 370, 981
- Virbhadra, K. S. 1997, *International Journal of Modern Physics A*, 12, 4831
- Virbhadra, K. S., & Ellis, G. F. 2002, *PhRvD*, 65, 103004
- Viththani, D. P., Joshi, A. B., Bhanja, T., & Joshi, P. S. 2024, *European Physical Journal C*, 84, 383
- Walsh, J. L., Barth, A. J., Ho, L. C., & Sarzi, M. 2013, *ApJ*, 770, 86
- Wielgus, M., Marchili, N., Martí-Vidal, I., et al. 2022, *ApJL*, 930, L19
- Wyman, M. 1981, *PhRvD*, 24, 839
- Yajima, H., & Tamaki, T. 2001, *PhRvD*, 63, 064007
- Yuan, F., & Narayan, R. 2014, *ARA&A*, 52, 529
- Yuan, F., Quataert, E., & Narayan, R. 2004, *ApJ*, 606, 894
- Zhu, L., Long, R. J., Mao, S., et al. 2014, *ApJ*, 792, 59



## APPENDIX

## A. POINT-LIKE SINGULARITY CLASSES

For P-type singularities, necessarily the divergence of higher-order derivative terms imply that  $N^2/r^2 B^2$  diverges, and thus all P-type singularities are P0.

We begin the proof of this by first looking at the case when  $B = 1$ , for which the order class is set by the lowest-derivative term of  $f/r^2$ ,  $f'/r$ , or  $f''$  that diverges. However, for a singularity to be anything other than P0-type,  $f$  must vanish at  $r = 0$  sufficiently rapidly. But in that case, by L'Hopital's rule,

$$\lim_{r \rightarrow 0} \frac{f'}{r} = 2 \lim_{r \rightarrow 0} \frac{f}{r^2}, \quad (\text{A1})$$

and thus it cannot be type P1. Similarly, if it is not P1,  $f'$  must vanish at  $r = 0$  but then,

$$\lim_{r \rightarrow 0} f'' = \lim_{r \rightarrow 0} \frac{f'}{r}, \quad (\text{A2})$$

and it cannot be P2. Thus, if a spacetime has a P-type singularity, has  $B = 1$ , and is not type P0, then it cannot be P1 or P2, yielding a contradiction. Because P-type singularities with  $B = 1$  exist, this immediately implies that all such singularities must be type P0.

We proceed with  $B \neq 1$  with similar line of argument. A P-type singularity that is not type P0 requires that  $N^2/B^2$  vanish at  $r = 0$  faster than  $r^2$ . But in that case,

$$\lim_{r \rightarrow 0} \frac{(N^2/B^2)'}{r} = \frac{1}{2} \lim_{r \rightarrow 0} \frac{N^2/B^2}{r^2}, \quad (\text{A3})$$

and the first 1st-derivative term must also be finite. If  $B$  is nonzero at  $r = 0$ , then,  $N^2$  must vanish at  $r = 0$  and by L'Hopital's rule,

$$\lim_{r \rightarrow 0} \frac{(N^2)'/r}{B^2} = \lim_{r \rightarrow 0} \frac{N^2/r^2}{B^2}. \quad (\text{A4})$$

If  $B$  vanishes at  $r = 0$  then  $N^2/r^2$  must also vanish at  $r = 0$  (which is a stronger statement than  $N^2$  vanishing), and the above still applies. Therefore, the second 1st-derivative term must also be finite. That is, if a spacetime is not type P0, it cannot be type P1.

We repeat this argument to show that a spacetime that is neither P0 nor P1, it cannot be P2. For the spacetime to not be type P1,  $(N^2)'$  must vanish at  $r = 0$  at least as fast as  $r$ , and therefore, by L'Hopital's rule,

$$\lim_{r \rightarrow 0} \frac{[(N^2)'/B]'}{B} = \lim_{r \rightarrow 0} \frac{[(N^2)'/B]/r}{B}, \quad (\text{A5})$$

which immediately implies that it cannot be type P2. Finally, as before, because P-type singularities exist, this immediately implies that all such singularities must be type P0.

## B. HORIZON APPROACH TIMESCALE

For comparison with the timescale estimates in [Section 3.2](#), here we make a similar estimate for general spherically symmetric, stationary black hole spacetimes. Such spacetimes are also described by [Equation 1](#), though defined by the vanishing of  $N^2$  at some radius  $r_h$ . Therefore, near this radius,

$$N^2(r) = (N^2)'(r - r_h) + \dots, \quad (\text{B6})$$

where  $(N^2)'$  is evaluated at  $r_h$  (suppressed for clarity). Thus, the timescale for reaching a radius  $r = r_h + s$  for small  $s$  is,

$$\begin{aligned} \Delta t_h &\approx \int_{r_h+s}^r dr \frac{eB}{(N^2)'(r - r_h)\sqrt{e^2 - V_{\text{eff}}^t}} \\ &\approx \frac{eB}{(N^2)'\sqrt{e^2 - V_{\text{eff}}^t}} \ln \left( \frac{r - r_h}{s} \right). \end{aligned} \quad (\text{B7})$$

As noted in [Section 3.2](#), this diverges logarithmically with  $s$ .

## C. EXCLUDING 4D EGBQ

Despite not being type-P0, the 4D charged Einstein-Gauss-Bonnet (4D EGBQ) naked singularity spacetime is still excluded for all parameter values ( $\gamma$ ,  $M$ , and  $Q$ ), and provides a natural example of the application of the general argument made here to beyond the P0 class.

For the 4D EGBQ spacetime,

$$N^2(r) = 1 + \frac{r^2}{2\gamma M^2} \left( 1 - \sqrt{D} \right), \quad (\text{C8})$$

where

$$D \equiv 1 + \frac{8\gamma M^3}{r^3} - \frac{4\gamma M^2 Q^2}{r^4}. \quad (\text{C9})$$

An event horizon exists when  $\gamma \leq 1 - Q^2/M^2$ , and possesses a naked singularity otherwise. The location of the singularity is set by the condition that  $D = 0$ , and is the largest positive root of

$$r_*^4 + 8\gamma M^2 r_* - 4\gamma M^2 Q^2 = 0. \quad (\text{C10})$$

Because  $\lim_{r \rightarrow \infty} D = 1$ , by definition  $D$  must be positive definite for all  $r > r_*$ , with two important consequences.

First, at  $r = r_*$ ,  $N^2(r_*) = 1 + r_*^2/(2\gamma M^2) > 1$ . A particle falling from infinity that is initially marginally bound has  $e^2 = m^2$ , and thus even with  $\ell = 0$ ,  $e^2 - V_{\text{eff}}^t(r_*, 0) < 0$  and there is an inner turning point for some  $r > r_*$ . For accreting particles on orbits with  $\ell \neq 0$ ,  $V_{\text{eff}}^t(r_*, \ell) > V_{\text{eff}}^t(r_*, 0)$ , and thus we concluded that an inner turning point always exists for physical accretion flows. The effective potential for an example

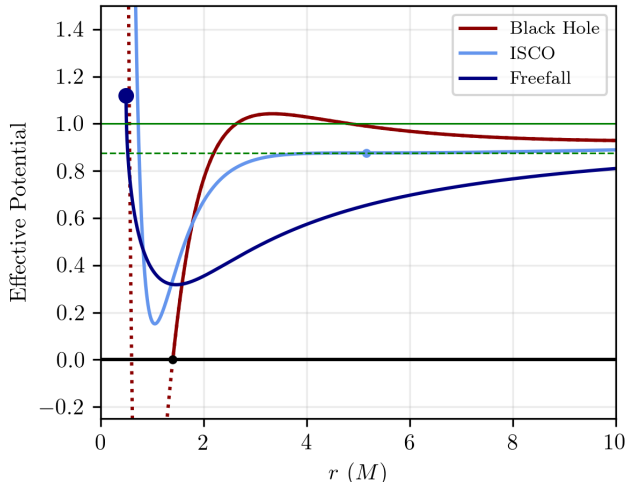


**Figure 4.** Effective potentials for three representative cases of the 4D EGBQ naked singularity with comparisons to the astrophysically relevant range of energies for accreting particles. Shown are  $V_{\text{eff}}^t$  for orbits with  $\ell = \sqrt{12}M$  in a black hole spacetime with  $(\gamma = 0.8, Q = 0.2)$ , dark red) with the radius of the horizon marked by the black point and the potential shown by a dotted line inside, orbits with  $\ell$  given by that at the outermost ISCO (light blue dot) in a naked singularity spacetime  $(\gamma = 1, Q = 0.2)$ , light blue), and orbits with  $\ell = 0$  in a naked singularity spacetime  $(\gamma = 1, Q = 1)$ , dark blue). For comparison, in green the values of  $e^2$  at the ISCO of the first singular spacetime (dashed) and  $e^2 = 1$  (solid) are indicated. While all examples have singularities at  $r_* > 0$ , only in the last case is the singularity visible in the plotted range (large dark blue point).

radial orbit is shown by the dark blue line in Figure 4, along with the  $e = 1$  line, illustrating this behavior.

Second,  $(N^2)'(r_*) < 0$ , and hence  $N^2(r_*)$  is a local maximum (in fact, it can be shown that  $\lim_{r \rightarrow r_*} (N^2)'(r) = -\infty$ ). Therefore, for accretion flows that effectively transport energy and angular momentum so that matter plunges from the outer innermost stable circular orbit (ISCO),  $e^2 = V_{\text{eff}}^t(r_{\text{ISCO}}, \ell_{\text{ISCO}}) < m^2$  and  $\ell_{\text{ISCO}} \neq 0$ . Hence, again, for such flows we generally have an inner turning point. The effective potential for such a case is shown by the light blue line in Figure 4, where  $\ell = 3.32M$  is the specific angular momentum at the ISCO, marked by the light blue dot.

Two practical effects may increase the specific energy of infalling orbits above unity. First, the accreting matter may begin far from the black hole with non-zero kinetic energy, e.g., the Bondi radius is not at infinity. However, such an increase is small – neither Sgr A\* nor M87\* are accreting from a distant, relativistically hot plasma, and in both sources the brightness temperatures measured by the EHT,  $\sim 10^{10}$  K, are less than the anticipated virial temperatures. Moreover, even were this

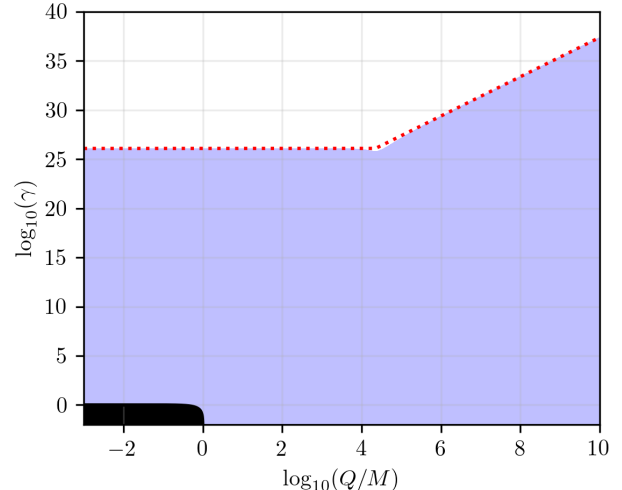


**Figure 5.** Excluded region (blue) in the  $\gamma$ - $Q$  parameter space of the 4D EGBQ naked singularity spacetime. The black region in the lower-left shows parameter values for which the 4D EGBQ metric describes a black hole. The dotted red line shows the approximation in Equation C12. Note that the axes are logarithmic.

the case, and some accreting particles were sufficiently to surmount  $V_{\text{eff}}^t(r_*, 0)$ , a significant fraction of particles would necessarily be launched on orbits with  $e < 1$ , and would therefore begin to form the inner settling flow, that when created would interact with and capture the energy from subsequently accreting particles of all masses.

Second, the act of heating the settling flow via accretion necessarily increases  $e$  locally. Again, this effect is small in Sgr A\* and M87\*, neither of which are expected to have relativistically hot settling flows (i.e., the  $kT_\infty \ll m_p c^2$ ). It remains formally possible for the thermal energy to be sufficient to raise the specific energy of the settling flow from the minimum to above  $V_{\text{eff}}^t(r_*, 0)$ . For small charges ( $(Q/M)^6 \ll 64\gamma$ ), this condition is dominated by the minimum of the effective potential, which for large  $\gamma$  occurs at  $r \approx \gamma^{1/3}M$  and is  $V_{\text{eff}}^t(r, 0) \approx 1 - \gamma^{-1/3}$ . For large charges ( $(Q/M)^6 \gg 64\gamma$ ), it is dominated by the effective potential at the singularity, which occurs at  $r_* \approx (4\gamma M^2 Q^2)^{1/4}$  and  $V_{\text{eff}}^t(r_*, 0) \approx \gamma^{-1/2}|Q/M|$ . Therefore, the energy gap to be overcome by the thermal energy is,

$$V_{\text{eff}}^t(r_*, 0) - V_{\text{eff}}^t(r, 0) = \begin{cases} \gamma^{-1/3} & (Q/M)^6 \ll 64\gamma \\ \gamma^{-1/2}|Q/M| & (Q/M)^6 \gg 64\gamma, \end{cases} \quad (\text{C11})$$

which implies that for the accretion-heating of the settling flow to drive matter into the singularity, the cou-

pling constant  $\gamma$  must satisfy,

$$\gamma \gg 10^{26} \begin{cases} \left(\frac{T_\infty}{10^4 \text{ K}}\right)^{-3} & \frac{Q}{M} < 2 \times 10^4 \left(\frac{T_\infty}{10^4 \text{ K}}\right)^{-1/2} \\ \left(\frac{T_\infty}{10^4 \text{ K}}\right)^{-2} \left(\frac{Q}{M}\right)^2 & \text{otherwise.} \end{cases} \quad (\text{C12})$$

This approximate constraint on  $\gamma$  matches that obtained by direct numerical computation, shown in [Figure 5](#), and effectively excludes the entirety of the physically credible parameter space.